Available online at www.sciencedirect.com
ScienceDirect
Catalysis Today 129 (2007) 59–68
CATALYSIS TODAY
www.elsevier.com/locate/cattod

Solar photocatalytic degradation of dichloroacetic acid with silica-supported titania at pilot-plant scale

Javier Marugán [a,1], Jose Aguado [a], Wolfgang Gernjak [b], Sixto Malato [b,*]

[a] Department of Chemical and Environmental Technology, ESCET, Universidad Rey Juan Carlos, C/ Tulipán s/n, 28933 Móstoles, Madrid, Spain
[b] Plataforma Solar de Almería, CIEMAT, Carretera Senés km 4, 04200 Tabernas, Almería, Spain

Available online 8 August 2007

Abstract

A multivariate analysis using experimental design techniques was performed to determine the effect of iron, hydrogen peroxide and titanium dioxide in the solar photodegradation of dichloroacetic acid in a combined TiO_2/photo-Fenton process. The study was carried out at pilot-plant scale, using TiO_2 supported on silica as the heterogeneous photocatalyst to facilitate separation of the solids after the reaction, and iron concentrations of less than 3 mg L^{-1} to avoid removal of iron from the effluent. The results show that iron is the most important factor influencing the reaction rate, which suggests that in strongly acidic solutions, the Fenton mechanism controls the process even at such low iron concentrations. Under these conditions, the expected synergism between TiO_2 and iron degradation pathways seems to be negligible compared to the antagonistic effect between hydrogen peroxide and TiO_2, which reduces the activity of the combined system. However, in the absence of hydrogen peroxide, the activity achieved by the combined Fe/TiO_2 system is similar to that of the photo-Fenton process, with the advantage that H_2O_2 is replaced by a reusable TiO_2-based catalytic material. Consequently, the analysis of pilot-plant operation economics took not only the degradation rate, but also the cost of chemicals into account.

Keywords: Photocatalysis; Photo-Fenton; Supported titania; Dichloroacetic acid; Experimental design; Optimization; Economic analysis

1. Introduction

The use of photochemical technologies has been shown to be a promising alternative for the detoxification of industrial effluents [1–3], especially from the environmental point of view [4]. Solar-driven advanced oxidation technologies such as semiconductor photocatalysis and photo-Fenton processes have demonstrated their suitability for the disposal of toxic and non-biodegradable pollutants resistant to conventional biological treatments [5–9].

One of these resistant chemicals is dichloroacetic acid (DCA), a widely used industrial pollutant also identified as an intermediate in the biological degradation pathway of many chlorinated hydrocarbons, and as one of the potentially carcinogenic disinfection by-products (DBP) formed in chlorination of water with traces of natural organic matter [10]. Since the early work of Ollis et al. [11], DCA has been used as the model pollutant by many research groups for the study of fundamental photocatalytic mechanisms [12], the influence of operating variables on solar photocatalytic processes [13,14], for kinetic modelling and photoreactor design [15], to compare the activity of new TiO_2 photocatalysts [16,17], and also to assess the activity of supported TiO_2 [18–20]. The use of supported titania has been shown to be a satisfactory way of recovering the catalyst after the reaction [21], one of the main problems hindering commercial application of TiO_2 photocatalysis in aqueous systems.

A previous work has studied Fe/TiO_2/pH interaction in the solar photodegradation of a model pesticide using TiO_2 supported on silica in the presence of excessive H_2O_2 [22]. Results showed that simultaneous semiconductor and photo-Fenton photocatalytic mechanisms were present. The reaction rates observed were controlled mainly by the iron chemistry, and pH was clearly the most influential variable, the reaction rate being fastest at acidic pH, as expected for a Fenton mechanism. However, at higher pH, the presence of TiO_2/SiO_2 photocatalysts produces a synergistic combination of the two degradation mechanisms, reducing the required amount of iron to below discharge limits.

* Corresponding author. Tel.: +34 950 387 940; fax: +34 950 365 015.
E-mail addresses: javier.marugan@urjc.es (J. Marugán), sixto.malato@psa.es (S. Malato).
[1] Tel.: +34 91 664 7466; Fax: +34 91 488 7068.

0920-5861/$ – see front matter
doi:10.1016/j.cattod.2007.06.054

This work focuses on the study of TiO_2/H_2O_2/Fe interaction in the solar photodegradation of DCA when Fe/H_2O_2 and silica-supported titania are used simultaneously in a pilot plant. Nogueira et al. [14] have reported on a small-scale multivariate analysis of the combined TiO_2/photo-Fenton process using powdered Degussa P25 TiO_2 and iron concentrations up to 60 mg L^{-1}. The purpose of the this study was to asses the activity and the synergies of the combined TiO_2/H_2O_2/Fe system at pilot-plant scale using SiO_2-supported TiO_2 photocatalysts to improve recovery of the solids after the reaction and iron concentrations of less than 3 mg L^{-1} to avoid iron removal. Experiments at acidic pH to maximize photo-Fenton efficiency and a multivariate analysis were performed to find out the effects of the three selected variables. Concentrations of TiO_2/SiO_2, iron and hydrogen peroxide were studied at five different levels (−1.68, −1, 0, +1 and +1.68), using a statistical approach to find the response surface of the photodegradation reaction rate. This method enables the influence of each variable to be determined along with any possible synergistic or antagonistic effects. The mathematical model obtained makes it possible to optimize pilot-plant operating conditions, minimizing the number of experiments required for process scale-up.

2. Experimental

2.1. Materials

Titanium dioxide was incorporated into a commercial porous silica (INEOS ES70Y, S_{BET} = 257 m^2 g^{-1}) using a sol–gel method. The synthesized photocatalyst consists of large approximately 50–70 μm silica particles with TiO_2 nanocrystals with a mean size of 7.2 nm homogeneously distributed over the SiO_2 surface. Further information on laboratory-scale synthesis, characterization and photocatalytic activity is available in a previous work [23].

Iron sulphate ($FeSO_4{\cdot}7H_2O$) and reagent-grade hydrogen peroxide (30 wt% aqueous solution) were used as the Fenton catalyst. No pH adjustment was required, as experiments were carried out at the natural acid pH of 5.0 mM dichloroacetic acid (DCA) reacting solution (∼2.4). Demineralised water came from the Plataforma Solar de Almería (PSA) distillation plant (conductivity < 10 μS cm^{-1}, Cl^- = 0.2–0.3 mg L^{-1}, NO_3^- = 0.5 mg L^{-1} and organic carbon < 0.5 mg L^{-1}).

2.2. Solar photodegradation experiments

Photocatalytic reactions were carried out under solar irradiation in compound parabolic collectors (CPC) at the Plataforma Solar de Almería (latitude 37°N, longitude 2.4°W). The twin pilot-plant systems each have a total volume of 35 L and 3.09 m^2 of irradiated surface. The 22 L irradiated aqueous suspension inside the solar collectors is recirculated through the system by a pump connected to a holding tank. A schematic of the experimental set-up can be found elsewhere [24]. At the beginning of the experiment, with collectors covered, all the chemicals and the TiO_2/SiO_2 material are added to the tank and mixed until constant concentration is achieved throughout the system. Usually 15 min are enough to assure the complete mixture of the reactor volume and then the photodegradation reaction is begun by removing the collector cover.

Samples were taken at preset time intervals and filtered through Millex-GN 0.2 μm syringe filters prior to analysis. Mineralization of DCA was monitored by measuring the total organic carbon (TOC) concentration remaining in the clear solution, using a Shimadzu 5050A TOC analyser calibrated with hydrogen potassium phthalate standard solutions. According to the accepted DCA photocatalytic degradation mechanism [11,16], TOC analysis provides information on the remaining amount of reagent due to the absence of any stable intermediates during the total mineralization process. In addition, chloride formation was measured by ion chromatography (IC) using a Dionex-600 (anions column IonPac AS14) with NaOH as the eluent. The mass balance between DCA degradation measured by TOC and the stoichiometric chloride formation detected by IC was achieved in all the experiments.

H_2O_2 concentration was monitored by iodometric titration, and dissolved iron concentration was determined by its colorimetric reaction with 1,10-phenanthroline after reduction of the iron(III) ions with ascorbic acid.

Solar ultraviolet radiation was measured by a global UV radiometer (KIPP & ZONEN, model CUV3) mounted on a south-facing platform tilted 37° (the same angle and orientation as the CPCs), which provides data in terms of incident W_{UV} m^{-2}, UV_G. As the irradiation conditions change during the experiments, to compare the results, the concentration profiles refer to the accumulated energy, $Q_{UV,n}$ (kJ L^{-1}), calculated as follows

$$Q_{UV,n} = Q_{UV,n-1} + \Delta t_n \overline{UV}_{G,n} \frac{A_{CPC}}{V_{TOT}} \quad (1)$$

where t_n is the experimental time for each sample, $\overline{UV}_{G,n}$ the average UV_G during Δt_n, A_{CPC} the collector surface (3.09 m^2) and V_{TOT} is the total plant volume (35 L).

A multivariate analysis of the influence of iron, TiO_2 and H_2O_2 concentrations on the photodegradation rate has been carried out, following a statistical approach based on a factorial design of experiments. It consisted of (i) eight experiments carried out at the −1/+1 levels of the three variables, (ii) three experiments at the centre point of the experimental domain (level 0 of the three factors) to determine the experimental error and check the linearity of results, and (iii) six experiments at the so-called star points where two variables are at the centre value and the third is set at two additional levels (−1.68/+1.68) above and below the maximum and minimum of the factorial design. These points are located on the axes of the coded variables at the same distance from the centre point as the factorial design experiments, defining a spherical experimental domain in which the same experimental error can be assumed. Table 1 summarizes the values and levels of the variables used to find a quadratic model by the response surface methodology [25]. Notice that the values of the factors were chosen in such a way that pure (Fe/H_2O_2) (Fe/TiO_2), and (TiO_2/H_2O_2) experiments were conducted at three of the star points.

Table 1
Experimental factor values and code levels

Factor	Code level				
	−1.68	−1	0	+1	+1.68
F1: TiO_2 concentration (g L^{-1})	0.0	0.06	0.15	0.24	0.30
F2: H_2O_2 concentration (g L^{-1})	0.0	0.2	0.5	0.8	1.0
F3: Iron concentration (mg L^{-1})	0.0	0.6	1.5	2.4	3.0

3. Results and discussion

Fig. 1 shows an example of the typical concentration profiles for total organic carbon (TOC), chloride and hydrogen peroxide versus incident energy accumulated in the system, $Q_{UV,n}$. Linear dependencies were found in all experiments, so the reaction rate can be described by fitting the experimental data to a zero order linear kinetics model.

Disappearance of DCA derived from the chloride formation profiles agrees with the values calculated from TOC evolution, indicating no significant disappearance of DCA due to adsorption and that the material balance is closed without the participation of any organic intermediates. Degradation therefore seems to take place through one of the following overall reactions, depending on the oxidizing species present in the medium:

$$CHCl_2{-}COOH + 2H_2O_2 \rightarrow 2CO_2 + 2H_2O + 2H^+ + 2Cl^- \quad (2)$$

$$CHCl_2{-}COOH + O_2 \rightarrow 2CO_2 + 2H^+ + 2Cl^- \quad (3)$$

Stoichiometric consumption of 2 mol of hydrogen peroxide per mol of DCA is derived from Reaction (2). This yields a value of 340 mg L^{-1} as the stoichiometric H_2O_2 required for total mineralization of the 5 mol_{DCA} L^{-1} solution. Fig. 1 shows that the actual consumption rate of H_2O_2 could be much higher than that of DCA degradation. Consequently, the ratio of the depletion rates of the two reactants is also of economic importance in evaluating reaction performance.

Table 2 shows the calculated DCA degradation rates and hydrogen peroxide consumption expressed in terms of $mol_{H_2O_2}/mol_{DCA}$. Although experiments are listed in a logical order to facilitate discussion, they were carried out in a random sequence to increase the statistical significance and avoid systematic errors.

Analysis of the experimental DCA photodegradation rates followed the steps below, as described previously [22]:

(i) The two-level factorial design consisting of Experiments 1–8 and the three replications of the centre point were done first. The estimated experimental error calculated from the standard deviation of these three replications and the Student's test parameter for a 95% confidence level and two degrees of freedom is 0.090 mol_{DCA} kJ^{-1}. With an average of 4.45 mol_{DCA} kJ^{-1} for the centre point experiments, the relative error is only 2%, certainly low for pilot-plant scale.

(ii) Second, model linearity is verified by calculating the curve as the difference between the average of the eight experiments of the factorial design and the average of the centre points. This was found to be 0.458 ± 0.11, which means there is a significant curve (above the corresponding error), so further experiments were conducted (Experiments 12–17) to include quadratic terms in the response surface equation.

(iii) Finally, a multiple linear regression was used to fit the experimental results to a 10-parameter model including the 3 effects of every variable, the 3 binary interactions, the 3 quadratic effects and an offset, neglecting the possible influence of XY^2-type and ternary interactions. The most significant effects were identified in the first fit, removing those with coefficients below the corresponding error. The reduction in the number of parameters makes the mathematical model more plausible, which can be quantitatively assessed using the Fisher value as derived from the ANOVA.

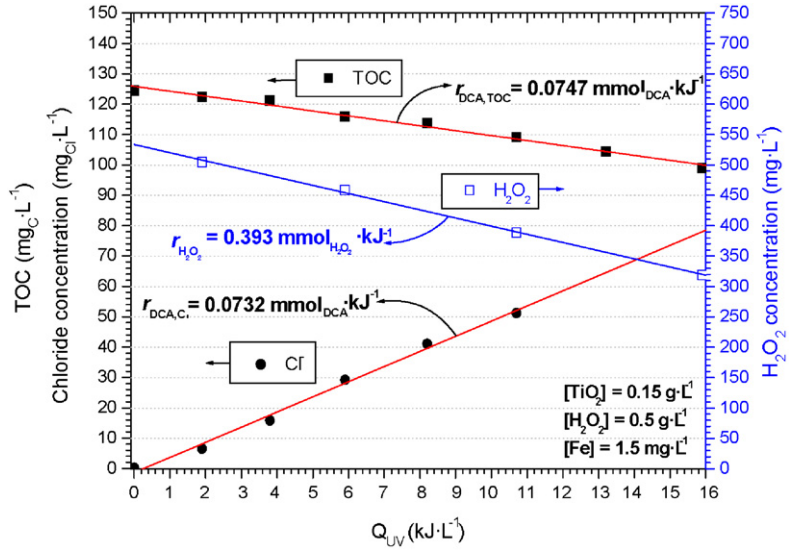

Fig. 1. Example of zero-order kinetics fit of hydrogen peroxide consumption and DCA photodegradation measured by TOC disappearance and chloride formation.

Table 2
Experimental results and DCA photodegradation rates predicted by the model

Experiment		Variable levels			$r_{DCA} \times 10^6$ ($mol_{DCA}\ kJ^{-1}$)			$r_{H_2O_2}/r_{DCA}$ ($mol_{H_2O_2}/mol_{DCA}$)		
No.	Code	$[TiO_2]$ ($g\ L^{-1}$)	$[H_2O_2]$ ($g\ L^{-1}$)	[Fe] ($mg\ L^{-1}$)	Experimental	Model prediction	Residue	Experimental	Model Prediction	Residue
1	−1/−1/−1	0.06	0.2	0.6	52.7	47.7	−4.9	2.74	3.14	0.39
2	+1/−1/−1	0.24	0.2	0.6	47.9	46.0	−1.9	3.81	4.03	0.22
3	−1/+1/−1	0.06	0.8	0.6	61.7	58.3	−3.5	6.52	7.25	0.73
4	+1/+1/−1	0.24	0.8	0.6	41.5	43.1	1.5	10.4	10.8	0.43
5	−1/−1/+1	0.06	0.2	2.4	80.6	79.4	−1.2	2.42	2.41	−0.01
6	+1/−1/+1	0.24	0.2	2.4	82.3	86.1	3.7	4.12	3.31	−0.81
7	−1/+1/+1	0.06	0.8	2.4	87.8	89.9	2.2	6.56	6.52	−0.04
8	+1/+1/+1	0.24	0.8	2.4	77.2	83.1	5.9	9.80	10.11	0.31
9	0/0/0	0.15	0.5	1.5	74.0	74.3	0.3	5.32	5.73	0.41
10	0/0/0	0.15	0.5	1.5	73.6	74.3	0.7	5.98	5.73	−0.25
11	0/0/0	0.15	0.5	1.5	74.8	74.3	−0.5	6.35	5.73	−0.63
12	−α/0/0	0.00	0.5	1.5	73.6	77.9	4.3	3.88	3.85	−0.02
13	+α/0/0	0.30	0.5	1.5	76.8	70.7	−6.0	7.46	7.61	0.15
14	0/−α/0	0.15	0.0	1.5	68.0	71.1	3.1	0.00	0.27	0.27
15	0/+α/0	0.15	1.0	1.5	80.7	77.5	−3.2	10.1	9.44	−0.71
16	0/0/−α	0.15	0.5	0.0	17.8	23.3	5.5	8.73	7.81	−0.92
17	0/0/+α	0.15	0.5	3.0	89.0	83.0	−6.1	6.14	6.62	0.47
χ^2							240.2			3.97

The final mathematical model that best fits the experimental response of the reaction rate of DCA solar photodegradation as a function of the concentration of TiO_2, iron and H_2O_2 is

$$r_{DCA}(\times 10^6\ mol_{DCA}\ kJ^{-1}) = 20.1 + 25.1[H_2O_2] + 44.2[Fe] - 124.96[TiO_2][H_2O_2] + 25.86[TiO_2][Fe] - 9.39[Fe]^2$$
$$(r^2 = 0.9568,\ \chi^2 = 240.2,\ F = 48.74,\ r_{DCA}\ \text{error} = 4.67 \times 10^{-6}\ mol_{DCA}\ kJ^{-1}) \quad (4)$$

where r^2 is the correlation coefficient, χ^2 the sum of quadratic residuals, F the F-value (from ANOVA) and r_{DCA} error is the response variable error.

Similarly, for the hydrogen peroxide consumption, the following mathematical model was obtained:

$$\frac{r_{H_2O_2}}{r_{DCA}}(mol_{H_2O_2}/mol_{DCA}) = 2.41 + 8.79[H_2O_2] - 2.38[Fe] + 25.0[TiO_2][H_2O_2] - 3.43[H_2O_2]^2 + 0.657[Fe]^2$$
$$(r^2 = 0.9703,\ \chi^2 = 3.97,\ F = 71.96,\ r_{H_2O_2}\ \text{error} = 0.60\ mol_{H_2O_2}/mol_{DCA}) \quad (5)$$

where r^2 is the correlation coefficient, χ^2 the sum of quadratic residuals, F is the F-value (from ANOVA) and $r_{H_2O_2}/r_{DCA}$ is the response variable error.

Table 2 gives the predicted DCA photodegradation rate and hydrogen peroxide consumption. To be sure that the response errors calculated for the models are statistically significant throughout the experimental domain, random distribution of residues must be verified and any systematic errors discarded. From the graphical analysis of the residuals after fitting (not shown), no tendency is observed in either the correlation of calculated and experimental values or any of the three variables studied. Consequently, polynomic expressions can be used to model the response surface well enough, and there is no need for variable transformation (e.g., logarithmic of the response), as when modelling the influence of variables causing differences of more than one order of magnitude in the experimental response [22].

Figs. 2–4 show the three-dimensional plots of both response surfaces at constant factor values. The spherical experimental domain defined by the factorial design has been projected over the surface marking the area in which the model could be properly applied and the area outside the projected circles in which the model has been extrapolated.

Prior to any mechanistic discussion of the response surfaces, some general considerations about the TiO_2/Fe/H_2O_2 photochemical system chemistry should be analyzed. The combination of TiO_2 photocatalysis and photo-assisted Fenton reaction significantly increases the number of homogeneous and heterogeneous catalytic reactions that take place in the reactor. In addition to the reactions of the two degradation mechanisms considered separately, the presence of TiO_2 provides a pathway for ferric iron reduction supplementing the light-activated reaction, which can boost the Fenton cycle and, thereby, hydroxyl radical generation [26,27]. On the other hand, the presence of ferric ions can improve charge separation on the TiO_2 surface by capturing the conduction band electron, stabilizing the valence band hole, and reducing the recombination rate [26]. Consequently, TiO_2/Fe combination could produce a synergistic effect, increasing the activity of both TiO_2 and Fenton hydroxyl radical generation mechanisms. A detailed analysis of the chemistry of the TiO_2/Fe/H_2O_2/UV system can be found elsewhere [22].

In view of the analysis in Figs. 2–4, it may be said that the iron concentration is the most influential DCA degradation rate

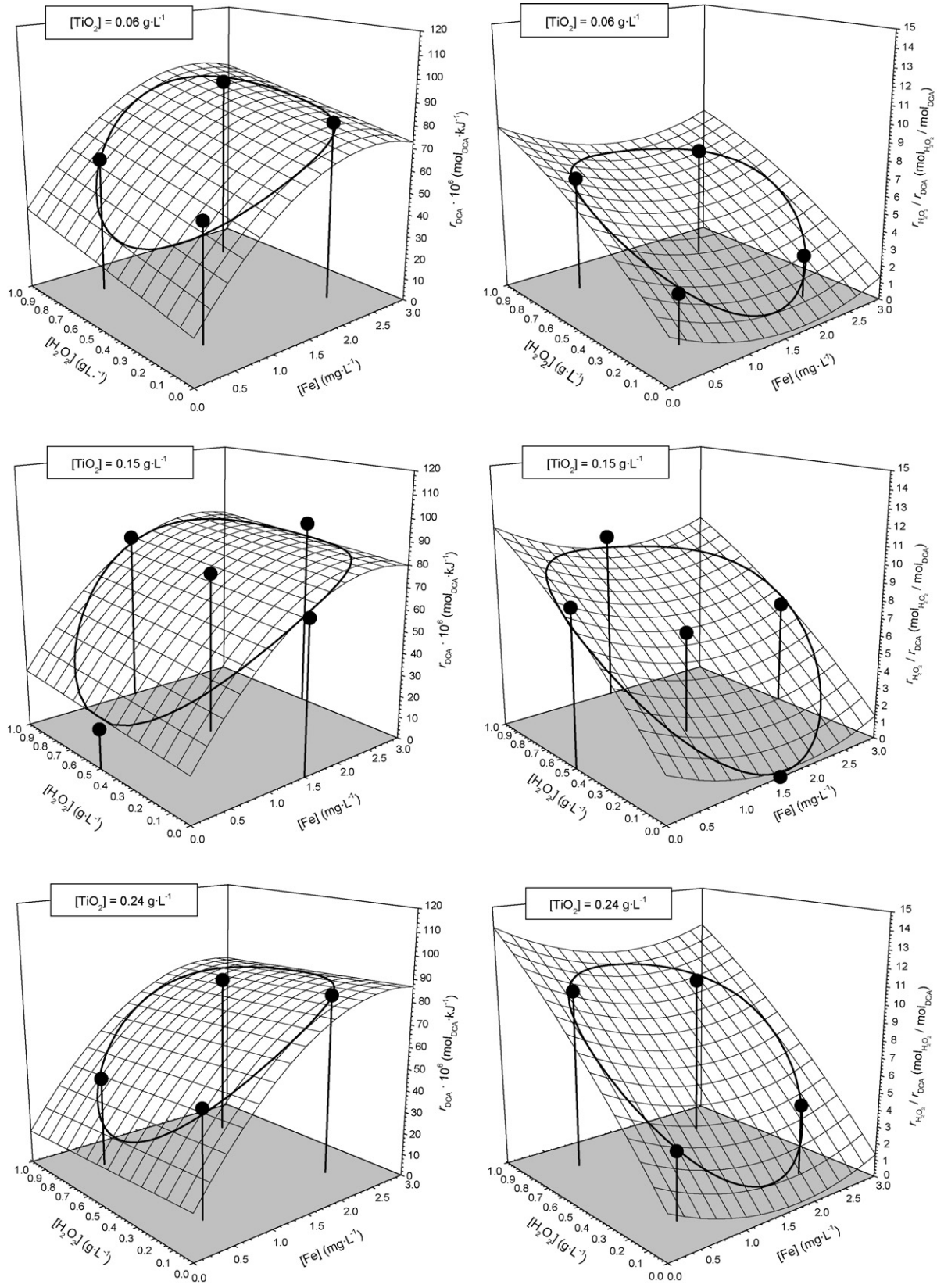

Fig. 2. 3D graphical representation of the response surfaces of DCA reaction rate and H_2O_2 consumption at the TiO_2 concentration −1, 0 and +1 code levels. (●) Represents the experimental points. The curve over the 3D surface is the projection of the experimental domain in which the model could be applied.

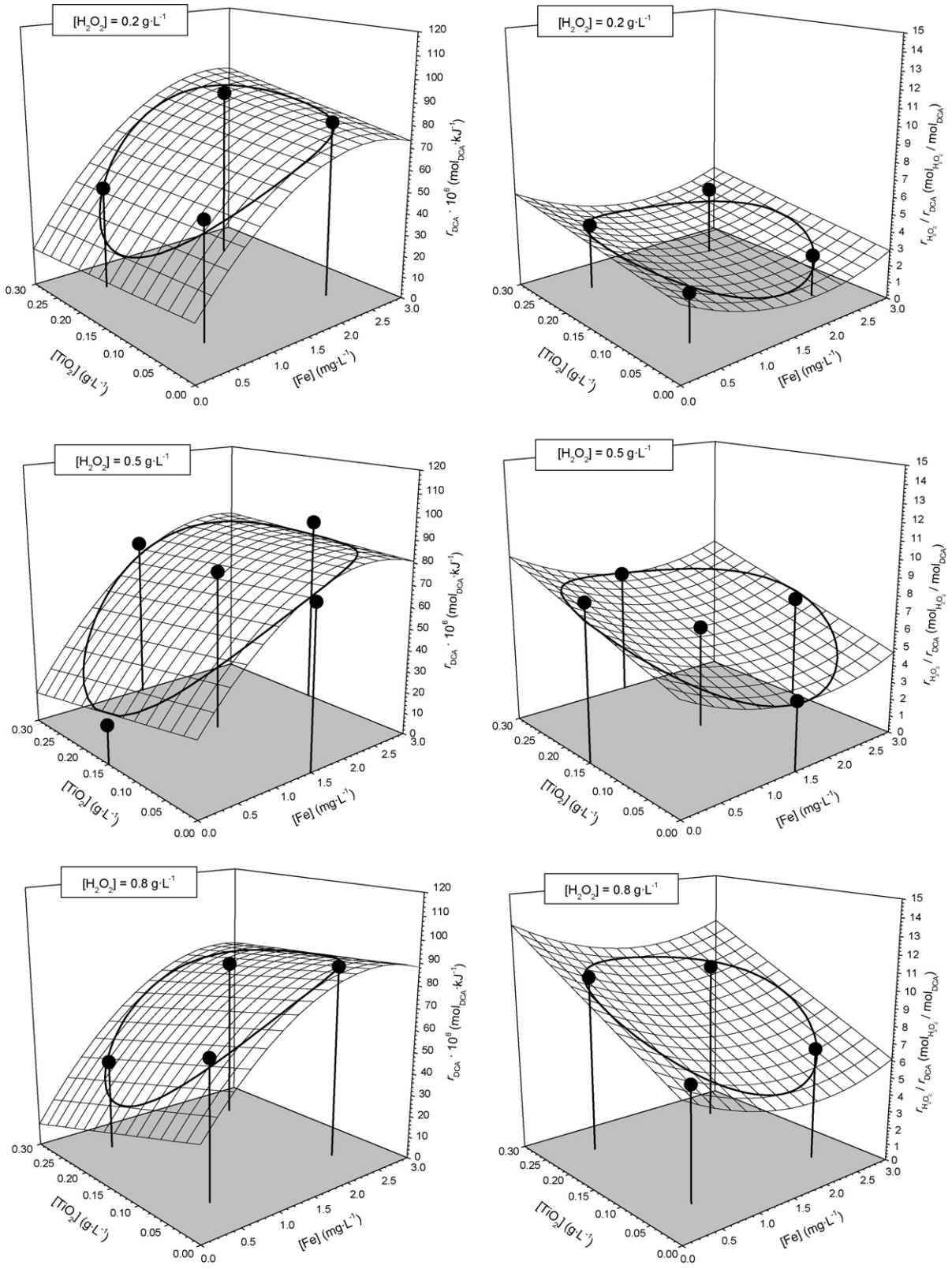

Fig. 3. 3D graphical representation of the response surfaces of DCA reaction rate and H_2O_2 consumption at the H_2O_2 concentration −1, 0 and +1 code levels. (●) Represents the experimental points. The curve over the 3D surface is the projection of the experimental domain in which the model could be applied.

factor. r_{DCA} increases with higher [Fe] significantly more than with $[H_2O_2]$ and $[TiO_2]$. Consequently, the overall degradation process seems to be controlled by the iron mechanism. The oxidation/reduction cycle can take place not only in the homogeneous phase but also on adsorbed iron. Heterogeneous processes could also be produced over iron hydroxides and oxides precipitated at higher pH, but usually at lower reaction rates [28]. Iron measurements confirmed that, in all the

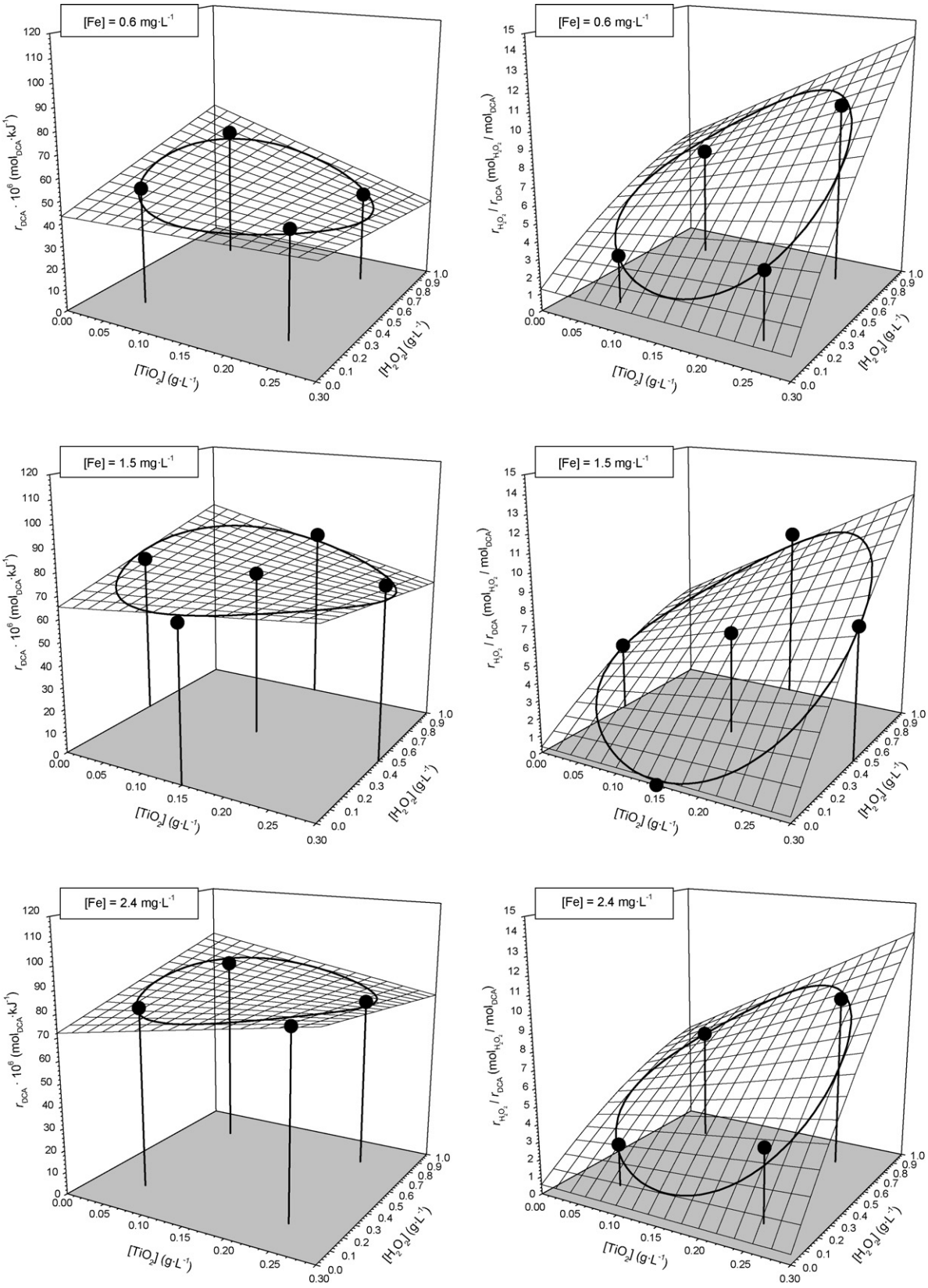

Fig. 4. 3D graphical representation of the response surfaces of DCA reaction rate and H_2O_2 consumption at the iron concentration −1, 0 and +1 code levels. (●) Represents the experimental points. The curve over the 3D surface is the projection of the experimental domain in which the model could be applied.

experiments, soluble species are mainly present as expected at the measured pH (1.9–2.4). Solution pH showed progressive acidification during irradiation as the reaction took place, due to the formation of HCl as a product of mineralization. This low pH is close to the optimum range for photo-Fenton. TiO_2 photocatalytic degradation of DCA has also been shown to be optimum at acidic pH values in the range in which DCA is dissociated ($pK_a = 1.29$) [20] and TiO_2 is positively charged (pH_{ZPC} 5.5–7.0 [29]). Moreover, close to pH 2, as is the case in this study, interaction with the silica support is also favored, as it could even be below the zero-charge point of silica (pH_{ZPC} 2.0–4.0 [29]).

Fig. 2 shows that at the lowest [TiO_2], the reaction rate seems to increase with higher [H_2O_2], whereas at the highest [TiO_2], the degradation rate is observed to decrease with increasing [H_2O_2]. Similarly, from the plots in Fig. 3, it may be concluded that an increase in titania concentration decreases r_{DCA} much more as the concentration of hydrogen peroxide increases. This antagonistic effect between [TiO_2] and [H_2O_2] is confirmed in Fig. 4, where it is clearly shown that at a constant iron concentration, the higher degradation rates are obtained at the maximum [H_2O_2] but minimum [TiO_2], and at the maximum [TiO_2] and minimum [H_2O_2]. The combination of high concentrations of both factors leads to results similar to when both of them are at their lowest levels. This negative effect can also be observed in Eq. (4), the mathematical expression of the response surface, where the product of both factors shows a negative coefficient with a high absolute value. From a mechanistic viewpoint, this negative interaction could be due to modification of the TiO_2 surface by the reaction with peroxide, or to more scavenging of hydroxyl radicals formed from the valence band holes than conduction band electrons, as previously suggested for pure TiO_2/UV/H_2O_2 systems [30,31]. H_2O_2 has two functions in the photocatalytic oxidation process. It accepts photogenerated electrons from the conduction band of the semiconductor, thus promoting charge separation, and it also forms OH radicals. As H_2O_2 is a better electron acceptor than Fe^{3+}, when H_2O_2 is at high concentration it impedes the reduction of Fe^{3+} by the photogenerated electrons of TiO_2. Under these circumstances the unique way of reducing Fe^{3+} is by solar photons. But if we increase at the same time the concentration of TiO_2, we are impeding the correct illumination of Fe^{3+}. Therefore, at high TiO_2 and H_2O_2 concentrations, the extension of the photo-Fenton mechanism is limited producing a decrease in the overall reaction rate. Moreover, when there is an excess of H_2O_2, it may react with TiO_2, and form peroxo compounds, which would also reduce the extension of the semiconductor mediated photocatalytic mechanism [32].

The factor that most influences the $r_{H_2O_2}/r_{DCA}$ ratio is the initial concentration of H_2O_2 itself. From Figs. 2 and 4 it may be seen that at constant titanium dioxide and iron concentrations, the increase in hydrogen peroxide leads to H_2O_2 consumption several times higher than the stoichiometric amount for mineralization according to Reaction (2). Fig. 4 also shows that a significant increase in the $r_{H_2O_2}/r_{DCA}$ ratio is observed when the TiO_2 concentration is increased at high [H_2O_2], confirming a waste of H_2O_2 in unproductive reactions with TiO_2 as mentioned above. As H_2O_2 is a reagent (and not a catalyst like Fe and TiO_2), the only important point to be considered is that its concentration is high enough so as not to limit the reaction. In this context, we propose automatic dosing in an attempt to keep it at a predefined concentration in order to maximize the reaction rate. On the other hand, it seems that efficient use of hydrogen peroxide is only slightly affected by the iron concentration. The $r_{H_2O_2}/r_{DCA}$ ratio is at a minimum at intermediate iron concentrations, and variation is not very significant.

Finally, the unexpected, almost negligible influence of hydrogen peroxide concentration on the DCA photodegradation rate is worth mentioning. With Fe/TiO_2 in the total absence of H_2O_2 (Experiment 14), r_{DCA} was only 16% lower than with 1.0 g L^{-1} of H_2O_2 (Experiment 15). These results suggest that hydrogen-peroxide-mediated degradation is not always what is mainly responsible for the disappearance of DCA in all cases. It might therefore be concluded that the main mechanism governing photodegradation is neither heterogeneous TiO_2 photocatalysis nor pure photo-assisted Fenton (Fe/H_2O_2) alone, but the Fe/TiO_2 combination. Měšťánková et al. [26] have reported that a very positive effect is achieved by adding iron to a TiO_2 photocatalytic process, especially at very low pH, such as in DCA degradation. A detailed explanation of the photochemical cycle of the combined iron–TiO_2 system can be found in their work. In fact, from an analysis of Eq. (4), it may be inferred that the effect of TiO_2 on the DCA degradation rate is not simple, but involves a negative interaction with H_2O_2 and a positive interaction with iron.

Summarising, results show that iron concentration controls the kinetics observed in the solar photodegradation of DCA even at concentrations as low as 1 mg L^{-1}. When titanium dioxide is present at low concentrations, the photo-assisted Fenton degradation pathway seems to drive the process. However, when titania concentration increases, instead of the global reaction rate increasing due to the above-mentioned synergistic effect, it seems to produce a small decrease in r_{DCA}. The reason is that a large part of the H_2O_2 is consumed in unproductive reactions with TiO_2, so that the mechanism responsible for degradation seems to be the photochemical iron–TiO_2 cycle proposed by Měšťánková et al. [26]. TiO_2 has the advantage of being a catalytic material that can be recovered and reused, in contrast to the expense associated with H_2O_2 consumption. On the other hand, TiO_2 usually causes more mechanical problems in the system due to abrasion, and requires further treatment of the water after the reaction for the separation of solids.

Pilot-plant performance optimization must therefore consider system economics. On one hand, a high degradation rate is desirable to reduce the costs of investment amortization, energy and labour. On the other hand, hydrogen peroxide consumption, as the major chemical cost, must be kept as low as possible. The cost of iron may be considered negligible (below 5×10^{-6} € mg^{-1} from $FeSO_4 \cdot 7H_2O$), and also the cost of TiO_2, as above 98% of it may be reused. A cost function

for the optimization procedure may therefore be defined as follows:

$$\text{cost}\,(€\,\text{mol}_{\text{DCA}}^{-1}) = C_{\text{time}}\,(€\,\text{kJ}^{-1})\left(\frac{1}{r_{\text{DCA}}}\right) + C_{\text{H}_2\text{O}_2}\,(€\,\text{mol}_{\text{H}_2\text{O}_2}^{-1})\left(\frac{r_{\text{H}_2\text{O}_2}}{r_{\text{DCA}}}\right) \quad (6)$$

A price of $C_{\text{H}_2\text{O}_2} = 0.0453\,€\,\text{mol}_{\text{H}_2\text{O}_2}^{-1}$ has been considered, taking a reference price of $0.4\,€\,\text{L}^{-1}$ of commercial H_2O_2 30 wt%. $C_{\text{time}} = 2.02 \times 0^{-4}\,€\,\text{kJ}^{-1}$ is the estimated cost of operating time, considering an average annual irradiation of 18.8 W m^{-2} (from historical data recorded at the Plataforma Solar de Almeria) and a cost of 600 € m^{-2} of solar collectors estimated from previous experience in scaling-up photocatalytic pilot plants to medium-sized plants 100–500 m^2, assuming 4380 h $year^{-1}$ and a 10-year amortization.

Application of the Newton optimizing algorithm to Eq. (6) in this experimental domain leads to the following values of the factors for which the lowest treatment cost is found:

- $[TiO_2] = 0.210$ g L^{-1} (codified level: 0.66).
- $[H_2O_2] = 0.122$ g L^{-1} (codified level: −1.26).
- [Fe] = 2.30 mg L^{-1} (codified level: 0.89).
- estimated cost: $2.49\,€\,\text{mol}_{\text{DCA}}^{-1}$ ($19.3\,€\,\text{kg}_{\text{DCA}}^{-1}$).

Fig. 5 shows the contour plots (curves of equal values on the response surface) at constant factor values corresponding to the point of minimum-cost operation. It can be seen that this point does not correspond to an absolute minimum. The extrapolation of the model predicts that a lower treatment cost can be achieved at higher concentrations of iron and titanium dioxide, and also by removing the titanium dioxide and using high concentrations of hydrogen peroxide. It is worth mentioning that the estimated cost associated with Fe/H_2O_2 treatment without TiO_2 is only slightly higher than Fe/TiO_2 without H_2O_2. The reason is that hydrogen peroxide only accounts for less than 4% of the estimated total cost, the amortization of the investment being the main factor. In any case, the goal of this work was not an accurate economic evaluation of the plant, but the identification of the main factors determining the cost of the treatment. Among the two factors considered, reagent and investment cost, the latter is by far the more important. This paper also shows how response surface methodology (RSM) can be applied to an approximate economic analysis based on process performance indicators (kinetics and reagent consumption as a function of process parameters). For a more rigorous analysis, accurate economic data, which are strongly dependent on the specific pilot plant and wastewater, are required.

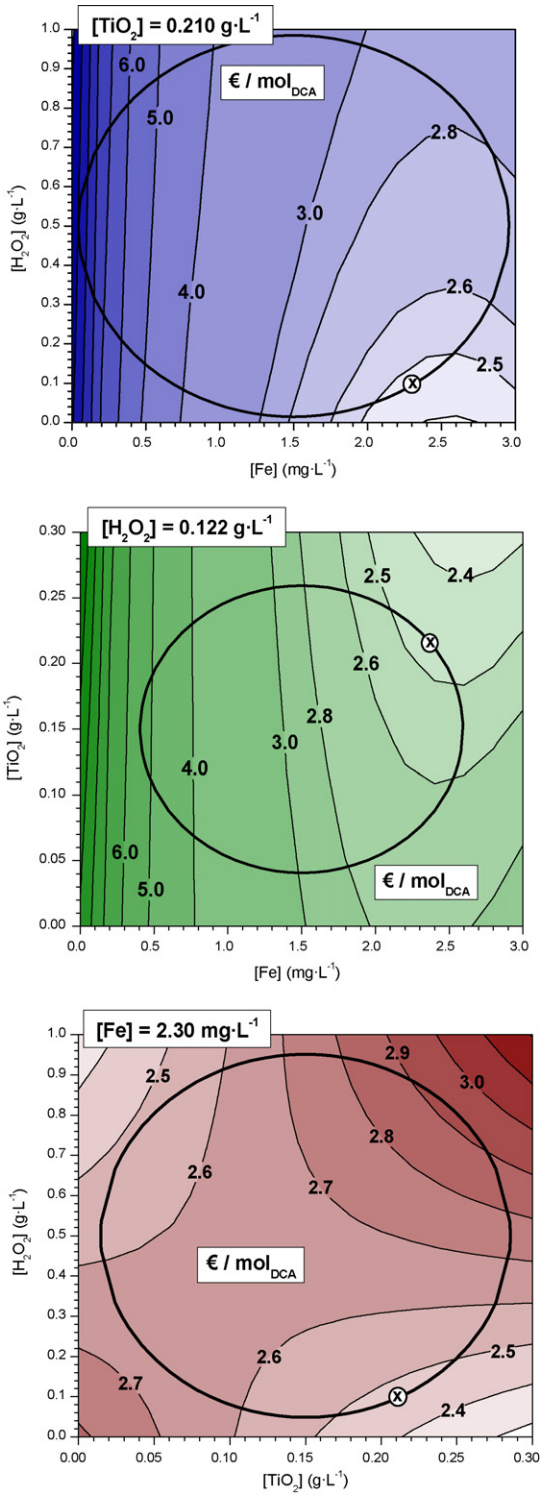

Fig. 5. Response surface contour plots for every factor at the optimal operating conditions. The circle represents the projection of the experimental domain in which the model could be applied.

4. Conclusions

The activity of the combined TiO_2/photo-Fenton photocatalytic system at strongly acidic conditions is controlled by the iron concentration even at concentrations below 3.0 mg Fe L^{-1}. The potential synergistic effect of TiO_2 and iron degradation pathways is overcome by an antagonistic effect between hydrogen peroxide and TiO_2 that reduces the activity of the combined system. At acidic pH values with low concentrations of titania, degradation is controlled by the photo-Fenton mechanism, whereas a photochemical Fe/TiO_2 cycle leads to similar activity at higher TiO_2 concentrations in

the absence of H_2O_2. These conditions seem to be of more economic interest, as TiO_2 can be recovered and reused, whereas the consumption of hydrogen peroxide is irreversible. Consequently, economic optimization of pilot-plant performance must take into account not only the conditions under which the reaction rate is highest, but also the lowest consumption of H_2O_2. A brief analysis of reagent and investment (depending on process kinetics) costs showed that in this case study the investment costs by far prevail over reagent costs. Hence, optimisation of process kinetics is of higher priority than optimising reagent consumption.

Acknowledgements

Financial support for this work was provided by the Spanish Ministerio de Ciencia y Tecnología through the program Consolider-Ingenio 2010 (project CSD2006-00044 TRAGUA) and Comunidad de Madrid through the program REMTAVARES S-0505/AMB/0395. Thanks are due to the whole Solar Chemistry Team at the Plataforma Solar de Almería for their help during the experiments.

References

[1] O. Legrini, E. Oliveros, A.M. Braun, Chem. Rev. 93 (1993) 671.
[2] U.S. Environmental Protection Agency, Handbook of Advanced Photochemical Oxidation Processes, EPA/625/R-98/004, 1998.
[3] S. Parsons (Ed.), Advanced Oxidation Processes for Water and Wastewater Treatment, IWA Publishing, 2004.
[4] I. Muñoz, J. Rieradevall, F. Torrades, J. Peral, X. Doménech, Sol. Energy 79 (2005) 369.
[5] S. Malato, J. Blanco, J. Cáceres, A.R. Fernández-Alba, A. Agüera, A. Rodríguez, Catal. Today 76 (2002) 209.
[6] I.K. Konstantinou, T.A. Albanis, Appl. Catal. B: Environ. 42 (2003) 319.
[7] M. Pera-Titus, V. García-Molina, M.A. Baños, J. Giménez, S. Esplugas, Appl. Catal. B: Environ. 47 (2004) 219.
[8] P.R. Gogate, A.B. Pandit, Adv. Environ. Res. 8 (2004) 501.
[9] P.R. Gogate, A.B. Pandit, Adv. Environ. Res. 8 (2004) 553.
[10] U.S. Environmental Protection Agency, Toxicological review of dichloroacetic acid, EPA 635/R-03/007, 2003.
[11] D.F. Ollis, C.Y. Hsiao, L. Budiman, C.L. Lee, J. Catal. 88 (1984) 89.
[12] S.T. Martin, C.L. Morrison, M.R. Hoffmann, J. Phys. Chem. 98 (1994) 13695.
[13] S. Malato, J. Blanco, A. Campos, J. Cáceres, C. Guillard, J.M. Herrmann, A.R. Fernández-Alba, Appl. Catal. B: Environ. 42 (2003) 349.
[14] R.F.P. Nogueira, A.G. Trovó, W.C. Paterlini, Water Sci. Technol. 49 (2004) 195.
[15] C.S. Zalazar, R.L. Romero, C.A. Martín, A.E. Cassano, Chem. Eng. Sci. 60 (2005) 5240.
[16] D.W. Bahnemann, S.N. Kholuiskaya, R. Dillert, A.I. Kulak, A.I. Kokorin, Appl. Catal. B: Environ. 36 (2002) 161.
[17] S. Sakthivel, M.C. Hidalgo, D.W. Bahnemann, S.-U. Geissen, V. Murugesan, A. Vogelpohl, Appl. Catal. B: Environ. 63 (2006) 31.
[18] R. Enriquez, B. Beaugiraud, P. Pichat, Water Sci. Technol. 49 (2004) 147.
[19] T.E. Doll, F.H. Frimmel, Acta Hydrochim. Hydrobiol. 32 (2004) 201.
[20] J. Marugán, D. Hufschmidt, G. Sagawe, V. Selzer, D. Bahnemann, Water Res. 40 (2006) 833.
[21] J. Aguado, R. van Grieken, M.J. López-Muñoz, J. Marugán, Catal. Today 75 (2002) 95.
[22] J. Marugán, M.J. López-Muñoz, W. Gernjak, S. Malato, Ind. Eng. Chem. Res. 45 (2006) 8900.
[23] R. van Grieken, J. Aguado, M.J. López-Muñoz, J. Marugán, J. Photochem. Photobiol. A: Chem. 148 (2002) 315.
[24] M. Kositzi, I. Poulios, S. Malato, J. Cáceres, A. Campos, Water Res. 38 (2004) 1147.
[25] G.E.P. Box, W.G. Hunter, J.S. Hunter, Statistics for Experimenters: An Introduction to Design, Data Analysis, and Model Building, Wiley, 1978.
[26] H. Měšťánková, G. Mailhot, J. Jirkovský, J. Krýsa, M. Bolte, Appl. Catal. B: Environ. 57 (2005) 257.
[27] J. Araña, O. González Díaz, M. Miranda Saracho, J.M. Doña Rodríguez, J.A. Herrera Melián, J. Pérez Peña, Appl. Catal. B: Environ. 36 (2002) 113.
[28] W. Feng, D. Nansheng, Chemosphere 41 (2000) 1137.
[29] K. Bourikas, C. Kordulis, A. Lycourghiotis, Environ. Sci. Technol. 39 (2005) 4100.
[30] P. Pichat, C. Guillard, L. Amalric, A.-C. Renard, O. Plaidy, Sol. Energy Mater. Sol. Cells 38 (1995) 391.
[31] D.D. Dionysiou, M.T. Suidan, I. Baudin, J.-M. Laîné, Appl. Catal. B: Environ. 50 (2004) 259.
[32] E.J. Wolfrum, D.F. Ollis, Hydrogen peroxide in heterogeneous photocatalysis, in: G. Helz, R. Zepp, D. Crosby (Eds.), Aquatic and Surface Photochemistry, Lewis Publ./CRC Press, 1994, pp. 451–465.